J. Hydrol. Hydromech., 68, 2020, 1, 70–82
DOI: 10.2478/johh-2019-0029
ISSN 1338-4333

sciendo Journal of Hydrology and Hydromechanics

Velocity profiles and turbulence intensities around side-by-side bridge piers under ice-covered flow condition

Mohammad Reza Namaee, Jueyi Sui*

Environmental Engineering Program, University of Northern British Columbia, 3333 University Way, Prince George, BC, Canada.
*Corresponding author. E-mail: jueyi.sui@unbc.ca

Abstract: Recent studies have shown that the presence of ice cover leads to an intensified local scour pattern in the vicinity of bridge piers. To investigate the local scour pattern in the vicinity of bridge pier under ice-covered flow condition comparing to that under open channel flow condition, it is essential to examine flow field around bridge piers under different flow conditions. In order to do so, after creation of smooth and rough ice covers, three-dimensional time-averaged velocity components around four pairs of bridge piers were measured using an Acoustic Doppler velocimetry (ADV). The ADV measured velocity profiles describe the difference between the velocity distributions in the vicinity of bridge piers under different covered conditions. Experimental results show that the vertical velocity distribution which represents the strength of downfall velocity is the greatest under rough covered condition which leads to a greater scour depth. Besides, results show that the turbulent intensity increases with pier size regardless of flow cover, which implies that larger scour depth occurs around piers with larger diameter.

Keywords: Bridge pier; Ice cover; Local scour; Acoustic Doppler velocimetry (ADV); Horseshoe vortex.

INTRODUCTION

Bridges constructed with elements within the boundaries of rivers are potentially exposed to scour around their foundations. If the depth of scour exceeds a critical value, instability and vulnerability caused by the scour will threaten the bridge foundation, which might possibly lead to critical issues such as bridge collapse, significant transport disruption and, in an extreme case, human casualty. Melville and Coleman (2000) studied 31 cases of bridge failures due to scour in New Zealand and concluded that, on average, one major bridge failure each year can be attributed to scour occurring around the bridge foundations. Wardhana and Hadipriono (2003) studied 500 cases of bridge structure failures in the United States between 1989 and 2000 and stated that the most common causes of bridge failure were either floods or scour. Sutherland (1986), in conjunction with National Roads Board of New Zealand, determined that of the 108 bridge failures recorded between 1960 and 1984, 29 could be attributed to abutment scour. Note that abutment scour is the removal of sediment around bridge abutments. Local scour around bridge foundations has been the focal point of many studies (Ahmed and Rajaratnam, 1998; Dey and Raikar, 2007; Ettema et al., 2011; Graf and Istiarto, 2002; Melville and Sutherland, 1988; Melville and Chiew, 1999; Sheppard et al., 2013; Williams et al., 2018; Williams et al., 2017; Wu and Balachandar, 2016; Wu et al., 2014, 2015a, b, c). Namaee and Sui (2019a) investigated the impact of armour layer on the scour depth around side-by-side bridge piers under ice-covered flow condition. Their study showed that the impact of armour layer is dependent on sediment type in which the piers are placed, and it increases as the sediment gets coarser regardless of pier size and pier shape.

Figure 1 illustrates mechanism of local scour around a submerged vertical cylinder adapted from Zhao et al. (2010). According to Williams et al. (2018), the scour commences in the region of the highest velocity in the vicinity of the separating streamline. The horseshoe vortex which forms at the pier face

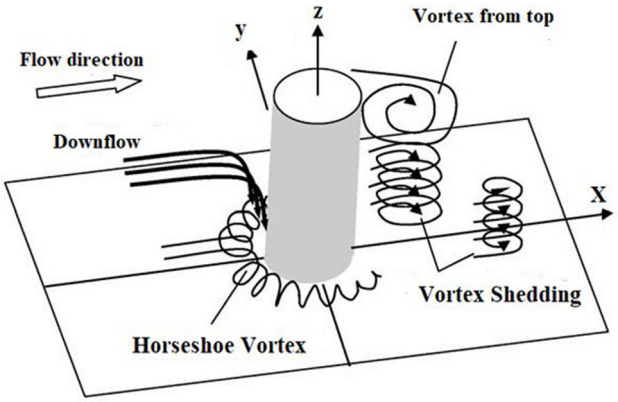

Fig. 1. Flow pattern around a submerged vertical cylinder (adapted from Zhao et al., 2010).

shifts the maximum downflow velocity closer to the pier in the scour hole. The downflow acts as a vertical jet to erode a groove in front of the pier. The eroded sand particles are carried around the pier by the combined action of accelerating flow and the spiral motion of the horseshoe vortex (Hafez, 2016). Melville and Coleman (2000) report a wake-vortex system which occurs behind the pier, acts like a vacuum cleaner sucking up bed material and carries the sediment moved by the horseshoe vortex system and by the downward flow to downstream of the pier (Vortex shedding in Fig. 1). However, wake-vortices are not normally as strong as the horseshoe vortex and therefore, are not able to carry the same sediment load as the horseshoe vortex does. Note that although a wider bridge pier results in a more accumulated armour layer around the bridge pier which ultimately decreases the scour depth, it results in a stronger horseshoe vortex at the pier face. Horseshoe vortex is the main driver in creation of local scour, and its impact is much stronger

than the impact of armour layer. According to Mohammed et al. (2007), a reduction of 15% in local scour depth can be obtained by using a pier having a streamlined shape instead of a squared-nose pier. This finding clearly shows that the pier shape factor has more impact on scour depth than that of the armour layer around bridge piers. Vijayasree et al. (2019) also stated that the scour process and the location of the maximum scour depth around the pier depended on shape of bridge pier. They claimed that a sharp nose with curved body is ideal for a bridge pier because of less scour around the pier. Gautam et al. (2019) investigated the variations in the turbulent flow field generated in the vicinity of a complex pier due to the presence of the pile-cap, and the results were compared with that of a simple pier without any pile-cap. It was concluded that the magnitude of the mean velocities, turbulence intensities and Reynolds shear stresses around a complex pier were less than those of the simple pier, indicating simpler fluid flow around the complex pier. Regarding scour at pile groups, Galan et al. (2019) revealed that depending on the submergence ratio as well as the angle of the piles with the approaching flow (skew-angle) and pile arrangements, the location of the maximum scour depths differs and it does not always occur at the first upstream pile. The experimental results of Zhao et al. (2010) which focuses on the local scour around a submerged pier showed that a decrease in pier height weakened the horseshoe vortex and vortex shedding which resulted in lower scour depths.

The velocity distribution in the vicinity of bridge piers is very important for the scouring process around bridge piers. Up to date, many researches regarding velocity distribution around bridge piers have been reported, such as Graf and Istiarto (2002); Unger and Hager (2007); Beheshti and Ataie-Ashtiani; (2009). Graf and Istiarto (2002) performed an experimental study of the flow pattern in the upstream and downstream plane of a cylinder positioned vertically in a scour hole. Detailed measurements were obtained by using an acoustic-Doppler velocity profiler (ADVP) in and around the scour hole. The results indicated that in the upstream reach of the cylinder, a strong vortex system was detected (horseshoe vortex) at the foot of the cylinder. In the downstream reach of the cylinder, a flow reversal existed towards the water surface. In their study, the results indicated the turbulent kinetic energy was very strong at the foot of the cylinder on the upstream side and in the wake behind the cylinder. Unger and Hager (2007) investigated the temporal evolution of the vertical deflected flow at the pier front and the horseshoe vortex inside the scour hole as it formed. Their work provided novel insight into the complex two-phase flow around circular bridge piers placed in loose sediment. A three-dimensional turbulent flow field around a complex bridge pier placed on a rough fixed bed was experimentally investigated by Beheshti and Ataie-Ashtiani (2009). Comparison of flow patterns with the observed scour map revealed that the scour patterns at the upstream and sides of the pier correlate well with the contracted flow below the pile cap. A flow field analysis around side-by-side piers with and without a scour hole was carried out by Ataie-Ashtiani and Aslani-Kordkandi (2012). They found that the streamwise velocity increased between the two piers. As a result, the maximum depth of the scour hole was approximately 15% greater than in the single-pier case. Kumar and Kothyari (2011) studied flow patterns and turbulence characteristics within a developing (transient stage) scour hole around both circular uniform and compound piers using an Acoustic Droppler Velocimeter (ADV). Their results for velocity, turbulence intensity and Reynolds shear stress around each of the piers along different vertical planes exhibited similar profiles with respect to flow depth. However, at certain locations close to the pier, significant changes occurred in the vertical profile of the flow parameters. While the observations made in the upstream planes revealed that within the scoured region, the bed shear stress was much smaller compared with the bed shear stress of the approach flow. Due to the difficulty in making velocity measurements under ice-covered conditions, nearly all the studies regarding velocity distribution around bridge piers have been carried out using open channel flow conditions. The number of studies on the flow field around both bridge abutments and bridge pier under ice-covered conditions is limited. Wu et al. (2015a) studied the effect of relative bed coarseness, flow shallowness, and pier Froude number on local scour around a bridge pier and reported the scour depth under covered conditions is larger compared to open channel flow conditions. It has been found that the presence of an ice cover alters the hydraulics of the channel by imposing an extra boundary to the water surface (Sui et al., 2010). Under ice-covered flow conditions, the velocity drops to zero at each boundary (ice-covered water surface and the bed) due to the no-slip boundary condition, resulting in a parabolic-shaped flow profile (Ettema, et al., 2000; Zabilansky et al., 2006). The maximum velocity occurs between the bed and the bottom of the ice cover and is dependent on the relative roughness of the two boundaries (Wang et al., 2008). Sui et al. (2010) showed that the upper flow is mainly influenced by the ice cover resistance while the lower flow is primarily impacted by the channel bed resistance. Wang et al. (2008) stated that the location of maximum velocity depends on the relative magnitudes of the ice and bed resistance coefficients. According to Wang et al. (2008), as the ice resistance increases, the maximum flow velocity will move closer to the channel bed. In terms of local scour depth, the severity of the local scour in the vicinity of a bridge's foundation intensifies during the freezing period when the water surface is covered with ice. The presence of ice has been found to increase local clear-water scour depth at bridge piers by 10%–35% (Hains and Zabilansky, 2004). In terms of transverse flow distributions and velocities of secondary currents, ice cover can impact flows in an existing thalweg, altering the position of the thalweg and changing the morphology of the stream which, in an extreme case, will lead to bank and bed erosion (Beltaos et al., 2007). Zabilansky et al. (2006) performed a series of flume experiments under smooth and rough ice cover conditions and found the maximum velocity for rough ice cover was 20 percent greater than for smooth ice cover. This statement was confirmed by Muste et al. (2000) who found the measured maximum velocity under smooth cover is located roughly at $0.8y_0$, while maximum velocity under rough cover is approximately located at $0.6y_0$, where y_0 represents the approaching flow depth. Overall, the rougher the ice cover, the closer the locale of maximum flow velocity to the bed. As a consequence, the bed shear stress increases which ultimately leads to increase in scour depths. In this study, a series of large-scale flume experiments were conducted to examine scour hole patterns along with scour hole velocity profile measurements around four side-by-side bridge piers under ice-covered and open channel flow conditions. The objective of this paper is mainly composed of two sections. In this section, it is explained how the existence of an ice cover changes the flow field in the vicinity of bridge piers. In the second section, it explains different scouring process resulted from different flow covers (open channel flow, smooth and rough ice-covered flows) by examining the 3D flow field velocity components especially downflow velocity which is proportional to the strength of horseshoe vortex.

METHODOLOGY

Experiments were carried out in a large-scale flume at the Quesnel River Research Centre of the University of Northern British Columbia, Canada. The flume was 38.2 m long, 2 m wide and 1.3 m deep. Fig. 2 shows a plan view and a side view of the experiment flume. The longitudinal slope of the flume was 0.2 percent. A holding tank with a volume of 90 m^3 was located at the upstream end of the flume to maintain a constant discharge during the experimental runs. To create different velocities, three input valves were connected to control the inlet volume discharge. Water level in the flume was controlled by the downstream tailgate. Two types of tailgate configurations (one-tailgate and two-tailgate configurations) were incorporated to produce a wide range of main channel approaching velocities. The range of flow depth was from 0.09 m to 0.137 m for the one-tailgate configuration and from 0.165 m to 0.28 m for the two-tailgate configuration. For the case of two-tailgate configuration, two pumps were employed for the lowest flow discharge while three pumps were employed to create the highest flow discharge. At the end of the holding tank and upstream of the main flume, water overflowed from a rectangular weir into the flume. Two sand boxes were constructed in the flume. Both had a depth of 0.3 m and were 10.2 m apart. The length of the sand boxes were 5.6 m and 5.8 m, respectively. Side-by-side cylindrical bridge piers with diameters of 60 mm, 90 mm, 110 mm and 170 mm were used. In terms of selection of sediment grain size, the mason, concrete and bedding mix sand types with median grain size D_{50} = 0.47 mm, 0.58 mm, 0.50 mm were selected. According to Hirshfield (2015), this selection was based upon the fact that the mason, concrete and bedding sands were the three most common sands mined from the surrounding quarries. Thus, our experiments have been conducted using these three sands in order to have the opportunity to meticulously compare our results of side-by-side bridge piers to those results of singular bridge pier of Hirshfield (2015) which is shown in Fig. 4.

The piers were spaced from each 0.50 m from center to center. Fig. 3 shows the piers and the space ratio (G/D) in which G is the distance between the piers and D is the pier diameter. The geometric channel aspect ratio (channel width/flow depth) in these series of experiments ranged from 7.14 to 22.2. The bridge pier spacing ratio G/D ranged from 1.94 to 7.33 (Fig. 3). In front of the first sand box, a 2D Flow Meter (Sontek, 2001) was installed to measure flow velocities and water depth. A staff gauge was also installed in the middle of each sand box to manually verify water depth. Styrofoam panels were used as ice cover across the entire surface of flume. Both smooth and rough

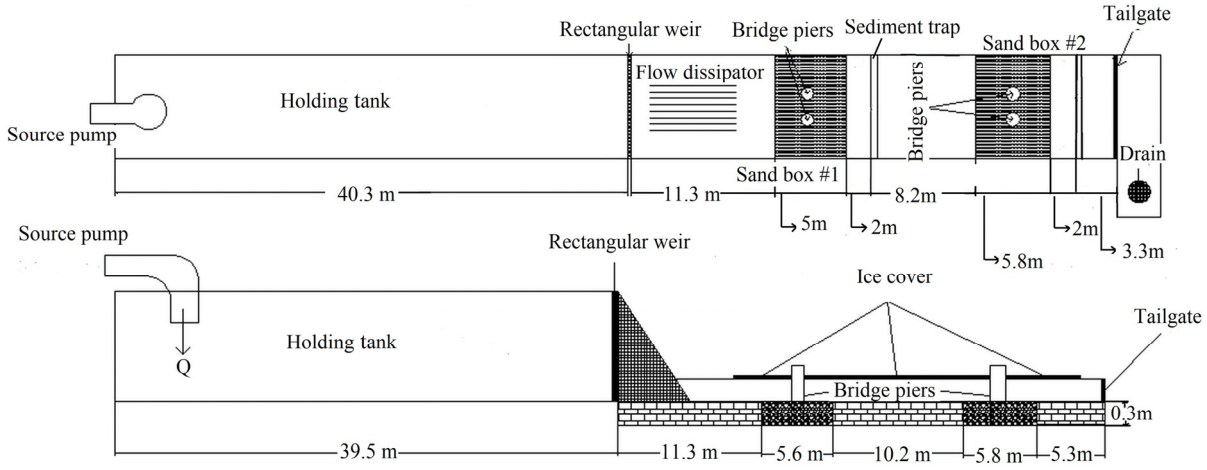

Fig. 2. Plan view and vertical view of experiment flume (Dimensions in m) (Namaee et al., 2019a).

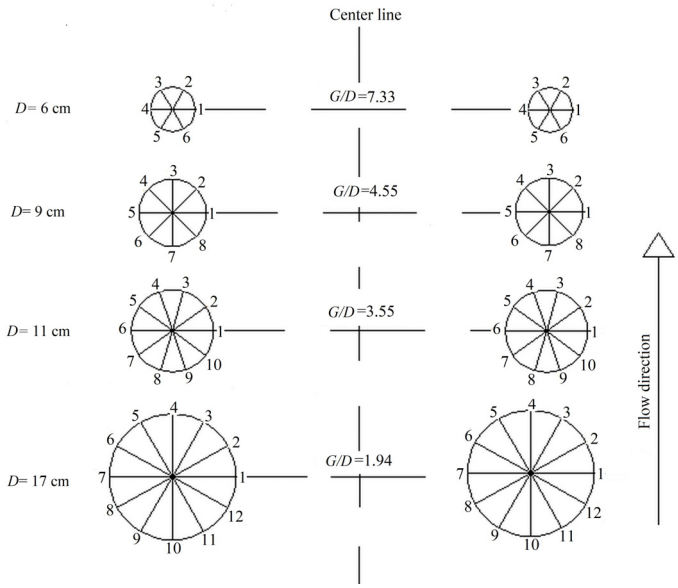

Fig. 3. The spacing ratio and measuring points around the circular bridge piers (Namaee et al., 2019a).

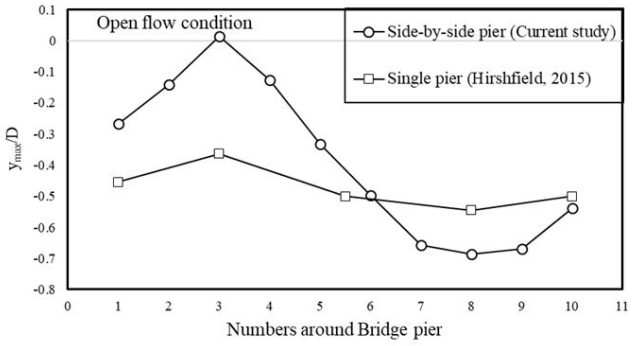

Fig. 4a. Scour depth around the 110-mm bridge pier for D_{50} = 0.47 mm type sediment under open flow.

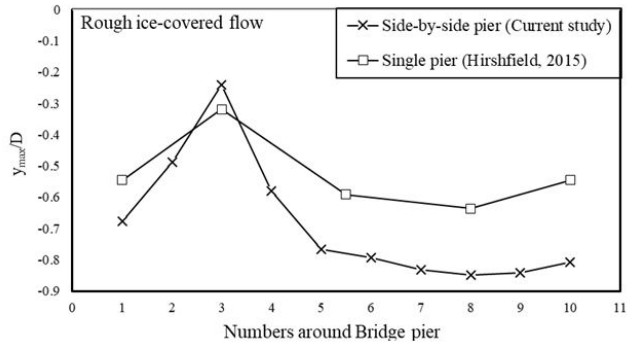

Fig. 4b. Scour depth around the 110-mm bridge pier for D_{50} = 0.47 mm type sediment under rough covered flow conditions using the highest flow discharge.

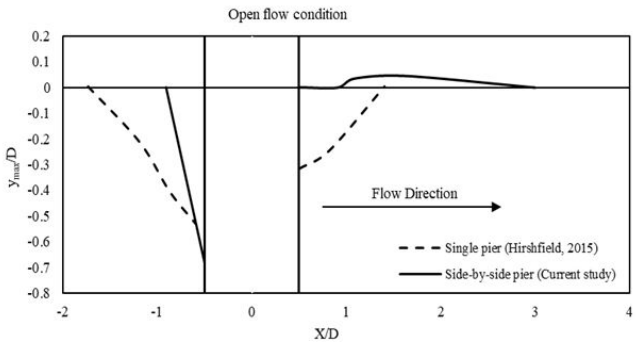

Fig. 4c. Cross-section of scour and depositional pattern at the upstream and downstream of the 110-mm bridge pier under open flow condition.

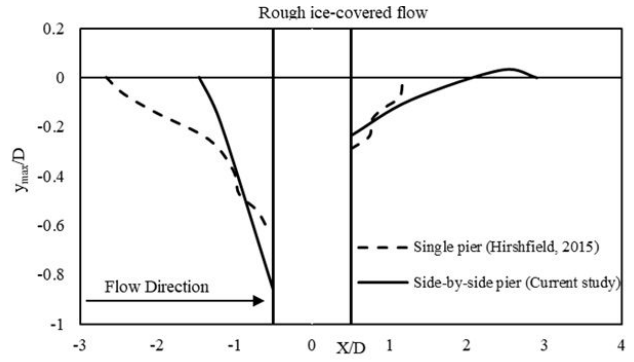

Fig. 4d. Cross-section of scour and depositional pattern at the upstream and downstream of the 110-mm bridge pier under rough covered flow conditions for D_{50} = 0.47 mm.

ice covers were simulated. The smooth cover was the smooth surface of the original Styrofoam panels while the rough cover was made by attaching small Styrofoam cubes to the bottom of the smooth cover. The dimensions of Styrofoam cubes were 25 mm × 25 mm × 25 mm and they were spaced 35 mm apart. The velocity field in the scour holes was measured using a 10-MHZ acoustic Doppler velocimeter (ADV). The sampling volume of the 10-MHz ADV is 100 mm from the sensor head. In a standard configuration, the sampling volume is approximately a cylinder of water with a diameter of 6 mm and a height of 9 mm. The ADV functions on the principal of a Doppler shift, measuring the phase change when the acoustic signal reflects off particles in the flow (Sontek, 1997).

In this study, the ADV measured the scour hole velocity profiles at approaching flow depths within 0.18–0.28 m range for four sets of bridge piers (60 mm, 90 mm 110 mm and 170 mm) when using the two-tailgate flume configurations for the highest and lowest levels of discharge. The positive direction of three-dimensional velocity components is shown in the coordinate system of Fig. 1. Scour hole velocity measurements for shallow flow depths (one-tailgate flume configuration) were inaccessible due to the limitations of the ADV in measuring shallow flow depths. Note that the difference between the water temperature measured by IQ with the water temperature measured by ADV was within 0.25 degrees Celsius. Velocity measurements were performed at one hour before the end of the experimental run (total test time = 24 hours) at which point the scour hole was fully developed and stabilized. For the purposes of these experiments, the streamwise velocity component is denoted as U_x, is the component in the direction of the flow, the span-wise velocity component is denoted as U_y is the component in the lateral direction and the vertical velocity component is denoted as U_z. Of note, a negative value of U_z means the velocity vector is directed downwards. To develop the three-dimensional velocity profiles, measurements were obtained at each point for 120 seconds. Of note, for velocity values very close to the channel bed, the presence of sediment affected the ADV velocity measurement, therefore, the velocity values are representative of sediment and water velocity as previous noted by Muste et al. (2000). The scour hole flow field was measured at 20 mm increments from the bottom of scour hole in front of the bridge pier up to free surface for each experimental run. In the ice-covered experiments, a part of the Styrofoam was cut to allow for the ADV to be positioned inside the flow for flow field measurements. Further, since the ADV measuring volume is located 100 mm from the probe head, the velocity profile for each channel condition does not continue up to the water surface. After the experiments were completed, collected data were analyzed to filter out for velocity spikes. Signal strengths and correlations are used principally to judge the quality and accuracy of the velocity data (Fugate and Friedrichs, 2002). In this study, data quality was defined based on signal-to-noise ratio amplitudes (SNR≥ 15) and correlation coefficient scores (≥ 70). In terms of uncertainty in velocity measurements, at a sampling rate of 25Hz and an SNR above 15, uncertainty due to Doppler noise can be estimated as 1% of the maximum velocity range (Sontek, 1997). Once ADV data is filtered for correlation, signal to noise ratios and data spikes, the velocity measurements were assumed to be accurate within 0.25 cm/s (Sontek, 1997). In total, 108 experiments (36 experiments for each sediment type) were conducted under open channel, smooth covered, and rough covered conditions. In terms of different boundary conditions (open channel, smooth, and rough covered flows), for each sediment type and each boundary condition, 12 experiments were carried out. In the preliminary stage of the

experiments, local scour around bridge piers was carefully observed for any changes in the scour depths. It was observed that after approximately a period of 6 hours, no significant change in scour depth was observed and scour hole equilibrium depth was achieved. The experiment was continued for 24 hours and again no obvious change in scour depth was observed. For the 110-mm bridge pier under open channel and ice-covered flow condition for the highest discharge, the experimental time was extended to 38 hours and there was not any significant change in scour depth between 24 hr. and 38 hr. experiments. Further, this agrees with a series of experiments by Wu et al. (2014), regarding local scour around a semicircular bridge abutment which determined the time for development of equilibrium scour depth as 24 hrs. After 24 hours, the flume was gradually drained, and the scour and deposition pattern around the piers was measured. Duration of experimental runs is one of important factors that affects the maximum scour depth. To explain it in more details, it is noteworthy to mention that one of the main criteria related to the bridge pier design is to predict the maximum scour depth where the bridge is constructed and subsequently to optimize the design of the foundation depth based. Clearly, the deeper the foundation placement, the higher cost for construction. However, the local scour process around bridge piers is a complex phenomenon which is dependent on many factors and is not easy to predict. For instance, the scour depth is dependent on the soil type that the piers are placed in (whether it is low-erodible or high-erodible), pier shape, pier spacing distance (our experiments showed that the closer the piers to each other, the larger the scour depth) and the existence of ice cover, to mention only a few. Most importantly, in most of the experiments including ours, the approaching velocity is kept as constant in order to simply the analysis of the experiments. However, in natural rivers, flow velocity is constantly changing, and thus the scouring process is a dynamic process. This means the prediction for local scour is even more difficult. On the other side, the scour process is much faster at the beginning and then slows down as the scour depth gets closer to the equilibrium scour depth. In our experiments, the majority of scouring process took place within the first 6 hours of the experiments. In the laboratory experiments of Vijayasree et al. (2019), it was observed that about 80% of the maximum scour depth occurred in the first 2 hours. Overall, local scour process is a very complex phenomenon and depends on many factors. That is the reason for attracting many

Table 1. Summary of experimental running conditions.

Run #	Cover	d (mm)	^{0}C (degrees)	y_0 (mm)	y_{max} (mm)	U (m/s)	U^* (m/s)	U/U^* –	Q (m^3/s)
1B	Open flow	60	11.83	250	22	0.11	0.20	0.56	0.056
2B	Open flow	60	11.62	110	35	0.18	0.14	1.30	0.040
3B	Open flow	60	11.45	280	25	0.17	0.21	0.81	0.094
4B	Open flow	90	11.83	200	35	0.13	0.18	0.74	0.054
5B	Open flow	90	11.62	90	60	0.25	0.13	1.96	0.045
6B	Open flow	90	11.45	230	68	0.20	0.19	1.05	0.093
7B	Open flow	110	11.50	242	25	0.12	0.19	0.60	0.058
8B	Open flow	110	11.83	100	71	0.28	0.13	2.09	0.056
9B	Open flow	110	11.72	253	75	0.20	0.20	1.05	0.101
10B	Open flow	170	11.50	250	24	0.12	0.20	0.59	0.059
11B	Open flow	170	11.83	100	45	0.18	0.13	1.35	0.036
12B	Open flow	170	11.72	270	48	0.16	0.20	0.77	0.084
13B	Smooth	60	11.62	250	29	0.12	0.15	0.82	0.061
14B	Smooth	60	11.59	110	35	0.17	0.10	1.68	0.037
15B	Smooth	60	11.55	260	42	0.17	0.15	1.16	0.090
16B	Smooth	90	11.62	200	31.2	0.15	0.13	1.13	0.060
17B	Smooth	90	11.59	100	64	0.23	0.10	2.40	0.046
18B	Smooth	90	11.55	240	68	0.20	0.14	1.38	0.096
19B	Smooth	110	11.59	243	42	0.10	0.14	0.68	0.048
20B	Smooth	110	11.10	90	78	0.21	0.09	2.29	0.038
21B	Smooth	110	11.57	255	80	0.20	0.15	1.44	0.102
22B	Smooth	170	11.59	260	29	0.09	0.15	0.63	0.049
23B	Smooth	170	11.10	105	48	0.15	0.10	1.55	0.032
24B	Smooth	170	11.54	250	49	0.18	0.15	1.20	0.089
25B	Rough	60	11.48	220	47	0.16	0.14	1.18	0.072
26B	Rough	60	11.45	100	55	0.17	0.10	1.76	0.034
27B	Rough	60	11.59	250	57	0.22	0.15	1.48	0.109
28B	Rough	90	11.48	220	67	0.14	0.14	0.99	0.061
29B	Rough	90	11.45	100	73	0.23	0.10	2.38	0.046
30B	Rough	90	11.59	230	85	0.20	0.14	1.37	0.090
31B	Rough	110	11.58	240	80	0.12	0.14	0.86	0.058
32B	Rough	110	11.61	90	92	0.20	0.09	2.22	0.037
33B	Rough	110	11.62	220	93	0.19	0.14	1.39	0.085
34B	Rough	170	11.58	220	49	0.12	0.14	0.86	0.053
35B	Rough	170	11.61	110	58	0.16	0.10	1.61	0.036
36B	Rough	170	11.62	280	61	0.17	0.16	1.08	0.093

researchers to do research work regarding the maximum scour depth around pier foundation.

To accurately read the scour depth at different locations and to draw scour hole contours, the outside perimeter of each bridge pier was divided between 6 and 12 labeled segments based on the diameter of the cylinder (Fig. 3). The measurement of scour hole was subject to an error of +/–0.3 mm. Table 1 tabulates the complete measured experimental data for D_{50} = 0.47 mm. In Table 1, y_{max} is the maximum scour depth, y_0 is the approach flow depth, U is the approaching flow velocity which is averaged over the flow depth, U^* is shear velocity also called friction velocity which is equal to $(gRS)^{0.5}$ (Namaee et al., 2017; Rickenmann and Recking, 2011), d is the diameter of the bridge piers, D_{50} is the medium grain size, Q is the volumetric flow discharge and ɵ is the flow (liquid) temperature. Of note, the maximum scour depth between left hand side and the right-hand side bridge piers were more or less identical. Note that this study is a part of a broad project in which impact of different parameters such as densimetric Froude number, armor layer, pier spacing and flow cover on the local scour in the vicinity of bridge piers has been painstakingly investigated (Namaee and Sui, 2019a; Namaee and Sui, 2019b and Namaee et al., 2019). Therefore, Fig. 2 and Fig. 3 are already refereed in those studies.

RESULTS AND DISCUSSIONS

Local Scour pattern around bridge piers

Fig. 4(a–b) shows scour depth around the 110 mm bridge pier and Figs. 4(c–d) compares the scour and depositional pattern upstream and downstream of the pier for D_{50} = 0.47 mm under open and rough flow conditions for the highest flow discharge, respectively. Fig. 4(a–d) also compares the scour depth of the present study with that of Hirshfield (2015) in which local scour around 110-mm single bridge pier under open and rough ice-covered flow conditions for D_{50} = 0.47 mm. Result of comparison reveals interesting information regarding how the local scour pattern around side-by-side bridge piers differs from that around singular bridge pier. As indicated in Fig. 4(a–b), regardless of the flow condition (either open flow or ice-covered flow conditions) and the number of piers, the maximum scour depth occurred at the upstream apex point of the pier face (point 8) where the horseshoe vortex and downflow velocity coexist and are the strongest. The least amount of scour occurred near point 3 which is diametrically opposed to point 8 and behind the pier. Further, Fig. 4 shows that the scour depth around the side-by-side pier configuration is deeper than that around the singular bridge pier in the study of Hirshfield (2015). According to Fig. 4b, sediment ridges have been developed downstream of the side-by-side bridge pier under all the flow cover conditions. However, for the single bridge pier, sediment ridges downstream of the pier were not reported by Hirshfield (2015). The reason is due to the confining effects of the side-by-side bridge pier when compared to the singular bridge pier which has resulted in greater scour depth and more developed sediment ridge at the downstream side of the bridge pier. This is in good agreement with result of Hodi (2009) that states, as the blockage ratio increases, larger amount of discrepancies will be developed in both scour depth and bed geometry. In the present study, regardless of flume cover, the maximum scour depths were always located at the upstream face of the pier. Since horseshoe vortex is stronger than the wake vortex, according to the description of Fig. 1, sediment deposition is likely to occur downstream of the pier in the form of a sediment ridge which is clearly shown in Fig. 4b. The scour pattern around the 110-mm bridge pier under highest flow discharge viewed from the top for D_{50} = 0.47 mm was mapped into Surfer 13 plotting software (Golden Software, 1999) as shown in Figs. 5(a–c) for open, smooth, and rough flow cover, respectively. Note that Namaee et al. (2019) already investigated the scour morphology around the 110-mm bridge pier under highest flow discharge for D_{50} = 0.47 mm. The reason why the same scour morphology is shown here is firstly because the aforementioned scour morphology is the most critical one in which the highest maximum scour depth was reached and secondly many more scour depths were collected for this scour morphology after the experiment to show a higher resolution scour morphology. According to Fig. 5, the deepest location of scour depth around the pier is clearly at the face of bridge pier and the location of deposition ridge is downstream of the pier which is densest and most widely spread for the rough ice-covered flow condition. The same pattern was observed for the other bridge piers regardless of sediment type and bridge pier diameter. It was experimentally noted by Qadar (1981) that the maximum value of scour depth should certainly be a function of the initial vortex strength. Therefore, the deepest scour depth, which is the result of a stronger vortex, should occur under the highest approaching velocity and roughest ice cover as observed in these experiments which clearly shows that the ice coverage increases the scour depth, and the rougher the ice cover, the greater the scour depth. Other factor which significantly impacts the local scour around side-by-side bridge piers compared to the singular bridge pier is the bridge spacing. Namaee and Sui (2019b) stated that the pier Reynolds number (Re_b) declines with increase in the pier spacing indicating that the strength of the horseshoe vortices reduces as the spacing distance between the side-by-side piers rises. Moreover, it was concluded that regardless of flow cover, the impact of ice cover on pier Reynolds number diminishes as the pier spacing distance increases. Note that the pier Reynolds number is defined as:

$$\mathrm{Re}_b = \frac{Ud}{\nu} \tag{1}$$

where, U is the average velocity of the approaching flow; d is the diameter of the bridge pier, and ν is the kinematic viscosity.

Flow velocity profiles

Scour hole velocity profiles for the streamwise (U_x) and vertical (U_z) velocity components under open, smooth and rough ice cover for all the piers size separately and under D_{50} = 0.47 mm for the lowest discharge is presented in Fig. 6. Fig. 7 shows scour hole velocity profiles for the streamwise (U_x) and vertical (U_z) velocity components distinguished by flow cover for all the pier sizes under D_{50} = 0.47 mm for the lowest discharge. Fig. 8 shows the vertical velocity distribution for the lowest discharge for the 90-mm bridge pier under rough ice-covered condition for the three D_{50}s. In order to be able to generalize the velocity profiles and to compare different velocity profiles under different flow cover, the depth of flow on the vertical axis has been non-dimensionalized by taking the ratio of vertical distance from bed (z) to approach flow depth (y_0). The streamwise scour hole velocity component (U_x) and the vertical scour hole velocity component (U_z) are also non-dimensionalized by the approaching flow velocity (U). Of note, the ADV location for the velocity measurement of all the experiments was set at 10 mm upstream of the pier face where the maximum scour depth occurred. The following outcome can be concluded from Figs. (6–8):

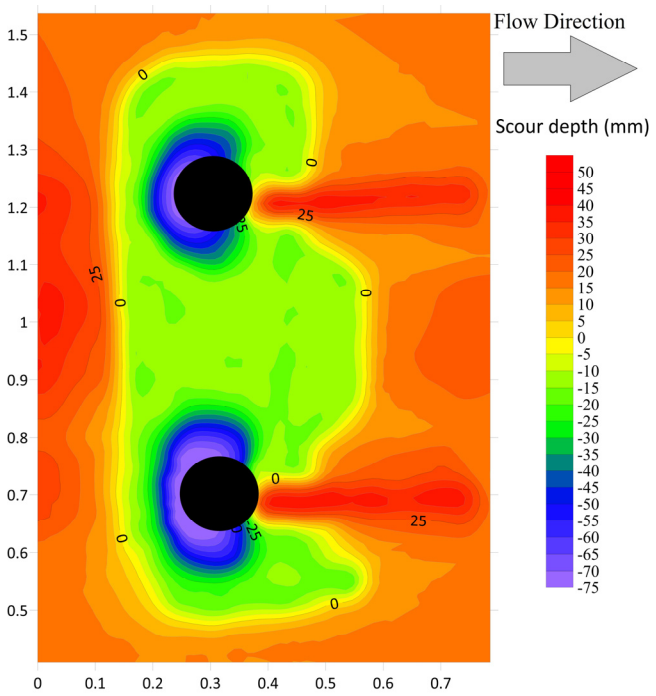

Fig. 5a. Scour pattern around the 110-mm bridge pier for D_{50} = 0.47 mm type under open for the highest flow discharge (Namaee et al., 2019).

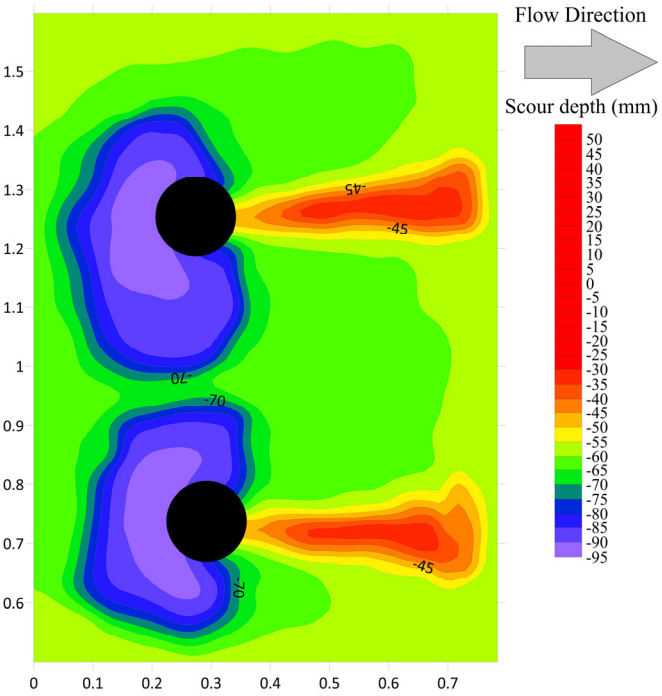

Fig. 5c. scour patterns around the 110-mm bridge pier for D_{50} = 0.47 mm type under rough for the highest flow discharge (Namaee et al., 2019).

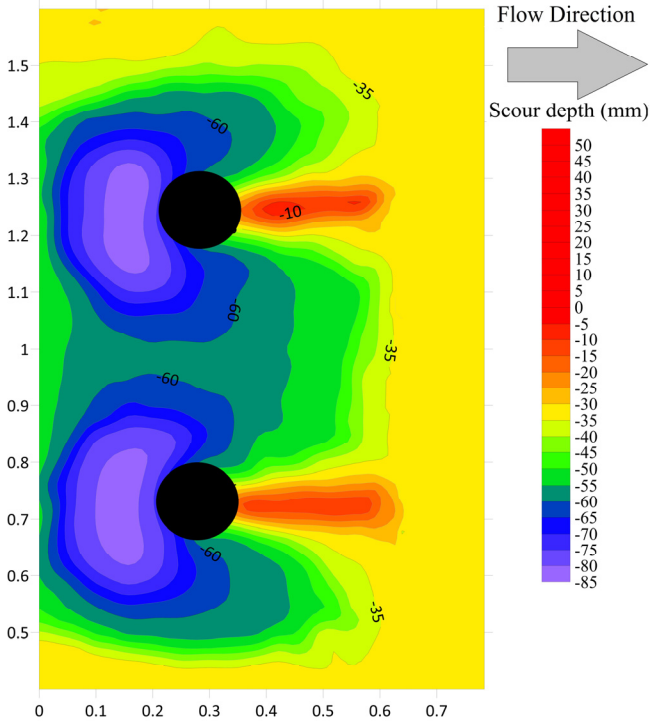

Fig. 5b. Scour pattern around the 110-mm bridge pier for D_{50} = 0.47 mm type under smooth for the highest flow discharge (Namaee et al., 2019).

1) The streamwise velocity distribution has a reversed C-shaped profile which begins from the scour hole up to the water surface. The same pattern was also reported by Hirshfield (2015) and Kumar and Kothyari (2011). In terms of velocity magnitude, the streamwise velocity for rough cover is generally greater than the scour hole velocity for smooth and open channel conditions. As expected, the magnitude of velocity is smallest in the scour hole and is the highest at the water surface. Furthermore, regardless of flow cover, pier size and sediment type, the values of the velocity component are mostly negative within the scour hole which is an indication of reversal flow happening due to the presence of horseshoe vortex which is strongest at the pier face. Moreover, for the 90-mm and 110-mm bridge piers, which were placed in the first sand box and were exposed to nearly the same flow depth and approaching flow velocity, the average value of U_x is higher for the 110-mm pier under all flow cover conditions. Similarly, for the 60 mm and 170 mm bridge piers which were placed in the second sand box and were exposed to nearly the same flow depth and approaching flow velocity, the average value of U_x is higher for the 170-mm pier under all flow cover conditions. In other words, these results indicate that the strength and intensity of the horseshoe vortex increased with pier size. Note that since the 90-mm and 110-mm bridge piers were placed in the first sand box and the 60 mm and 170 mm bridge piers were placed in the second sand box, the ADV measurements were done in both of the sandboxes.

2) Within the scour hole upstream of the pier, the most significant feature is the appearance of down-flow velocities in the vertical direction due to obstruction of the flow by the pier. It is represented by negative and values and is highly significant in terms of scour hole development. In terms of flow cover, it is obvious the value of U_z is the largest under rough ice cover. The downward velocity originates from the horizontal curvature of the streamline in front of the pier and the reduction of velocity near the bed by friction. Downward velocity intensifies the horseshoe vortex at the pier face and can effectively speed up the process of scour hole development, which in an extreme case, leads to bridge failure. Generally, considering the absolute value of U_z, the value of U_z diminishes from the channel bed toward the scour hole. From the channel bed toward the free surface, U_z values tend to move toward zero or the positive direction which implies that downflow velocity vectors are changing their direction and diminishing as they get closer to free surface which causes the velocity profile to have a parabolic shaped profile.

3) Under the same flow cover and flow condition, the larger pier yielded the larger values of the streamwise and vertical velocity values. However, these values are larger under rough ice-covered flow conditions. The larger scour hole velocity under rough ice cover justifies the findings of greater pier scour depth.

4) The vertical velocity distribution exhibits the same pattern for the three sands as seen in Fig. 8. According to the figure, the finest sediment (D_{50} = 0.47 mm), has a greater velocity magnitude and, consequently, a deeper scour depth. In addition, the location of maximum velocity under the finest sediment is closer to the bed which has resulted in stronger horseshoes vortices.

Table 2 represents the location of maximum velocity based on z/y_0 for different flow cover. Of note, the velocity profiles were measured before the cylinder inside the scour hole in the upstream region. According to Table 2, the location of maximum velocity under rough ice cover is closer to the bed which is in good agreement with the findings of Zabilansky et al. (2006) and Muste et al. (2000).

Fig. 9 shows scour hole velocity profiles for the lateral velocity component (U_y) distinguished by flow cover for all the pier size (D_{50} = 0.47 mm). As indicated by Fig. 9, there is not any meaningful pattern in the lateral velocity components due to high turbulence of flow in this direction.

Fig. 10a shows the vertical velocity component (U_z) for the 60- and 170-mm bridge piers (bridges in the second sand box) from the scour hole up to the maximum velocity point under open, smooth and rough-covered flow covers, while Fig. 10b shows U_z of the 90- and 110-mm bridge piers (bridges in the first sand box) from the scour hole up to the maximum velocity point under open, smooth and rough-covered flow covers.

Table 2. Location of maximum velocity based on (z/y_0) values according to flow cover.

Flow cover	Stage of maximum velocity (z/y_0)
Open channel	0.25
Smooth cover	0.15
Rough cover	0.10

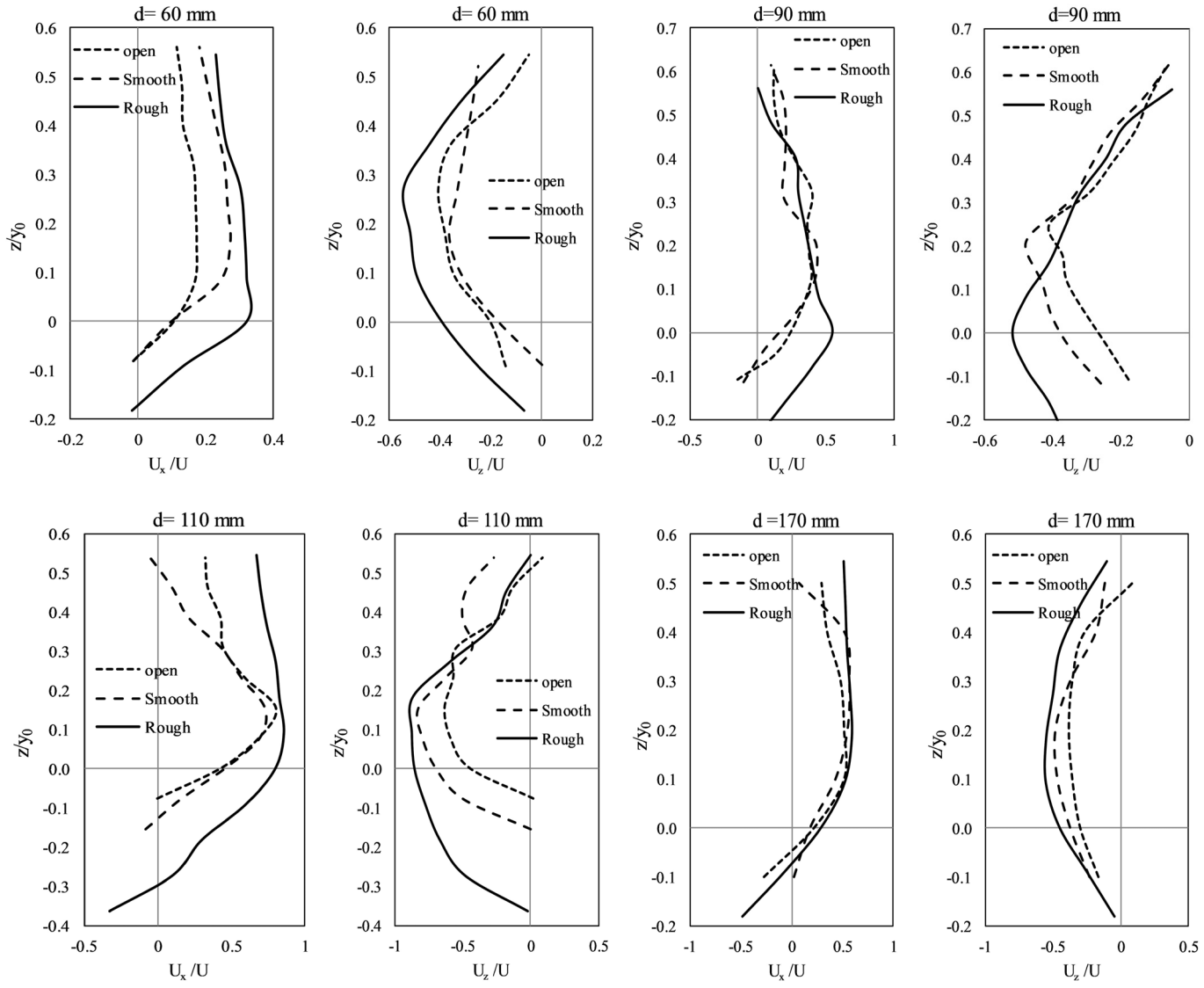

Fig. 6. Scour hole velocity profiles for the streamwise (U_x) and vertical (U_z) velocity components under open, smooth and rough ice-cover distinguished by the pier size and under D_{50} = 0.47 mm for the lowest discharge.

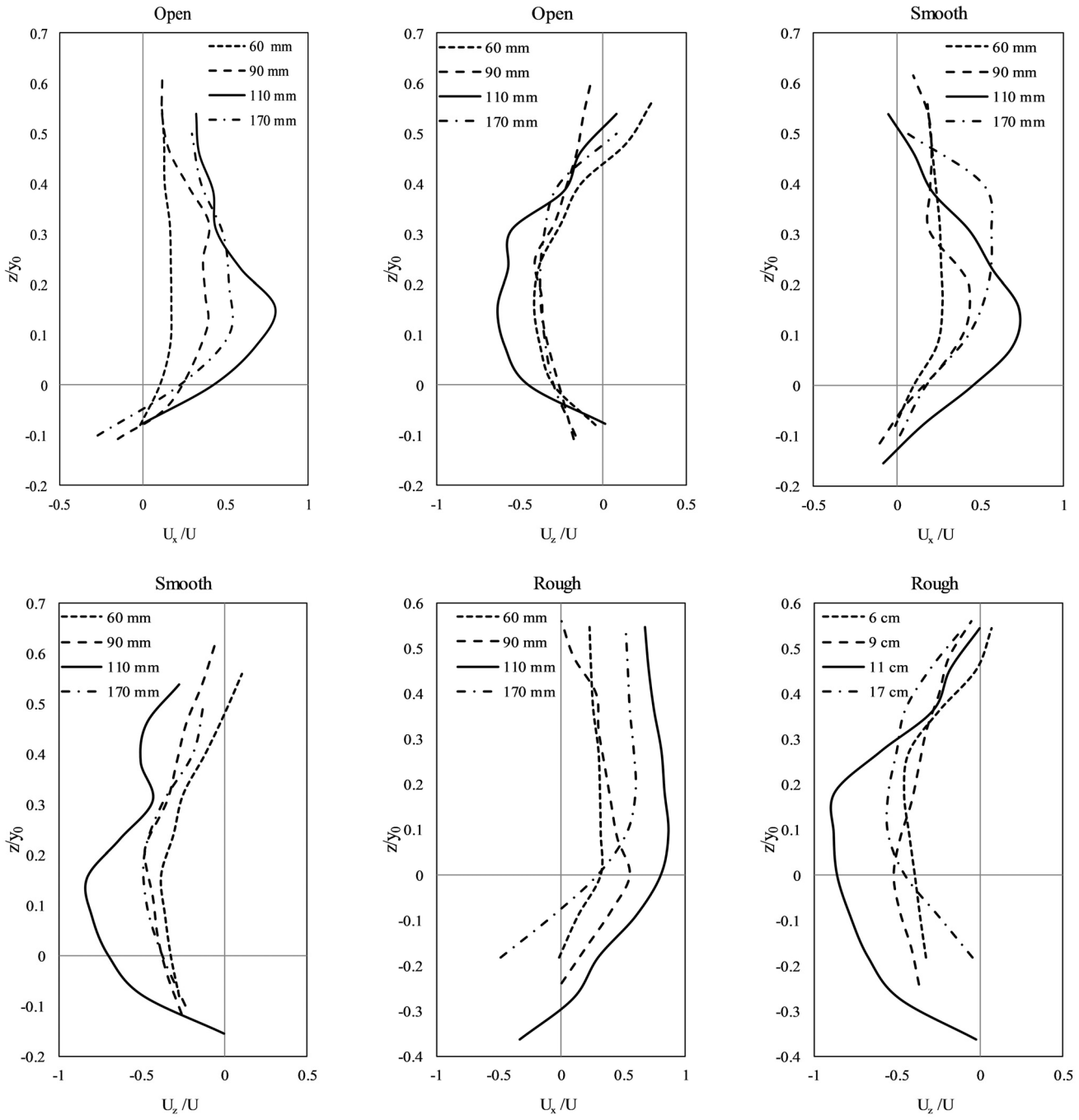

Fig. 7. Scour hole velocity profiles for the streamwise (U_x) and vertical (U_z) velocity components distinguished by flow cover for all the pier size and under D_{50} = 0.47 mm for the lowest discharge.

As mentioned before, the location of maximum velocity depends on the relative magnitudes of the ice and bed resistance coefficients and the rougher the ice cover, the closer the location of the maximum velocity to the channel bed. Therefore, the magnitude of vertical velocity is generally higher near the channel bed under rough flow cover compared to open channel flow cover. According to Figs. 10(a–b), location of the maximum velocity is closer to the bed under ice-covered condition which is in good agreement with previous findings. Since there was not any significant change from the maximum location of the vertical component of velocity *(U_z)* up to the free surface, a general linear relationship is developed for all the bridge piers under open channel and ice-covered flow conditions in Fig. 10c which reads as follows:

$$\frac{z}{y_0} = 0.5816\left(\frac{U_Z}{U}\right) + 0.5503 \tag{2}$$

Of note, due to the limitations of ADV in measuring the full vertical velocity profile, there is no data in the upper portions of the depth. Since the measurement of flow velocity is located at 10 cm beneath the measuring head of the 10 MHz ADV, the Sontek's 16 MHz micro ADV is recommended since the measuring head of the Sontek's 16 MHz micro ADV is smaller in size which also has less impact on the flow field around the scour depths. The velocity magnitude is calculated for the lowest discharge of D_{50} = 0.47 mm and are presented in Fig. 11.

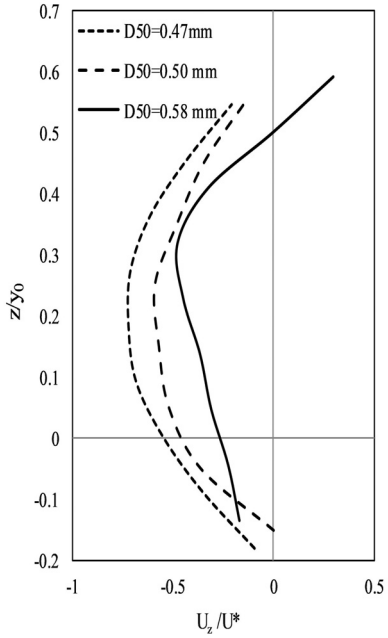

Fig. 8. The vertical velocity distribution for the lowest discharge for the 90-mm bridge pier under rough ice-covered condition for the three values of D_{50}.

The results indicate regardless of flow discharge and pier size, the velocity magnitude is highest for rough cover. For the 90-mm pier and 110-mm pier which were placed in the first sand box and were under nearly the same flow conditions, the larger pier has resulted in larger values of the velocity magnitude which implies that the strength and intensity of horseshoe vortex increases with pier size. The stronger horse vortex has also resulted in deeper scour depth for 110-mm bridge pier. The same trend can be seen for the 60-mm piers and 170-mm piers which were placed in the second sand box.

Turbulence intensities and turbulent kinetic energy (TKE)

In terms of ice-covered flow condition, the formation of a stable ice cover almost doubles the wetted perimeter compared to open channel conditions. This alters the hydraulics compared to an open channel by imposing an extra boundary to the flow, causing the velocity profile to be shifted towards the smoother boundary (channel bed) and adding to the flow resistance. Since the near-bed velocity is higher under ice-covered conditions, a higher shear stress is exerted on the riverbed (Sui et al., 2010; Wang et al., 2008). As the near bed velocity increases, the kinetic energy exerted on the bed increases correspondingly. An increase in kinetic energy affects the capacity of flow in terms of sediment transport rate. To determine turbulence intensities along with turbulent kinetic energy, the root-mean-square of the turbulent velocity fluctuations about the mean velocity are calculated. The root mean squares of the stream-wise, cross-stream, and vertical velocities for each time series were used to estimate TKE. The same unstructured turbulent intensities pattern was also observed by other studies such as Muste et al. (2000) and Robert and Tran (2012). Fig. 12 shows TKE values for all the piers for D_{50} = 47 mm for the lowest discharge. Note that since the profiles of turbulent intensities showed a rather similar pattern to TKE, only the result of TKE are shown. The following observations can be obtained:

1) Regardless of flow cover, the vertical turbulent intensity is highest just over the channel bed and diminishes towards the flow surface. According to Muste et al. (2000), observing the highest value of turbulent intensity near the bed is due to the highest rate of sediment movement near the bed. Muste et al. (2000) also concluded the turbulent intensities are relevant to sediment transport as the strength of the turbulence will affect sediment suspension.

2) The vertical turbulent intensity for the rough flow conditions is greater than those for open channel and smooth ice-covered flow conditions. As the turbulent intensity in the vertical direction is higher under the rough ice-covered flow

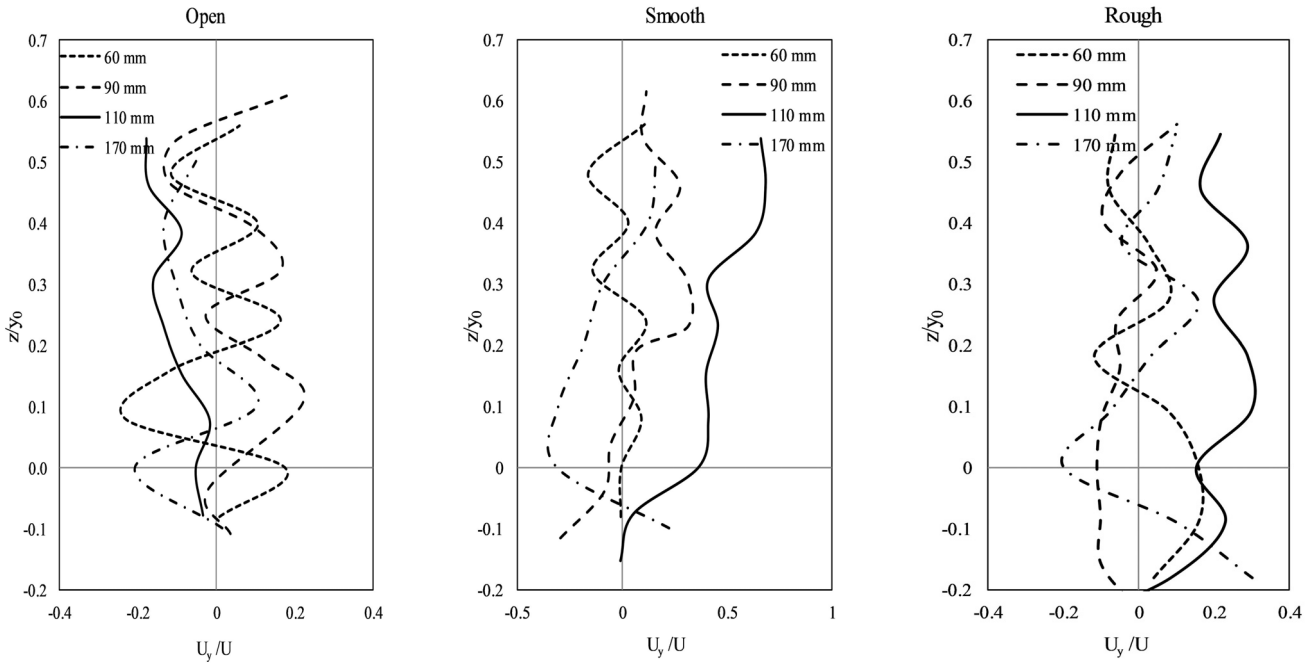

Fig. 9. Scour hole velocity profiles for the lateral (U_y) velocity component distinguished by flow cover for all the pier size and under D_{50} = 0.47 mm for the lowest discharge.

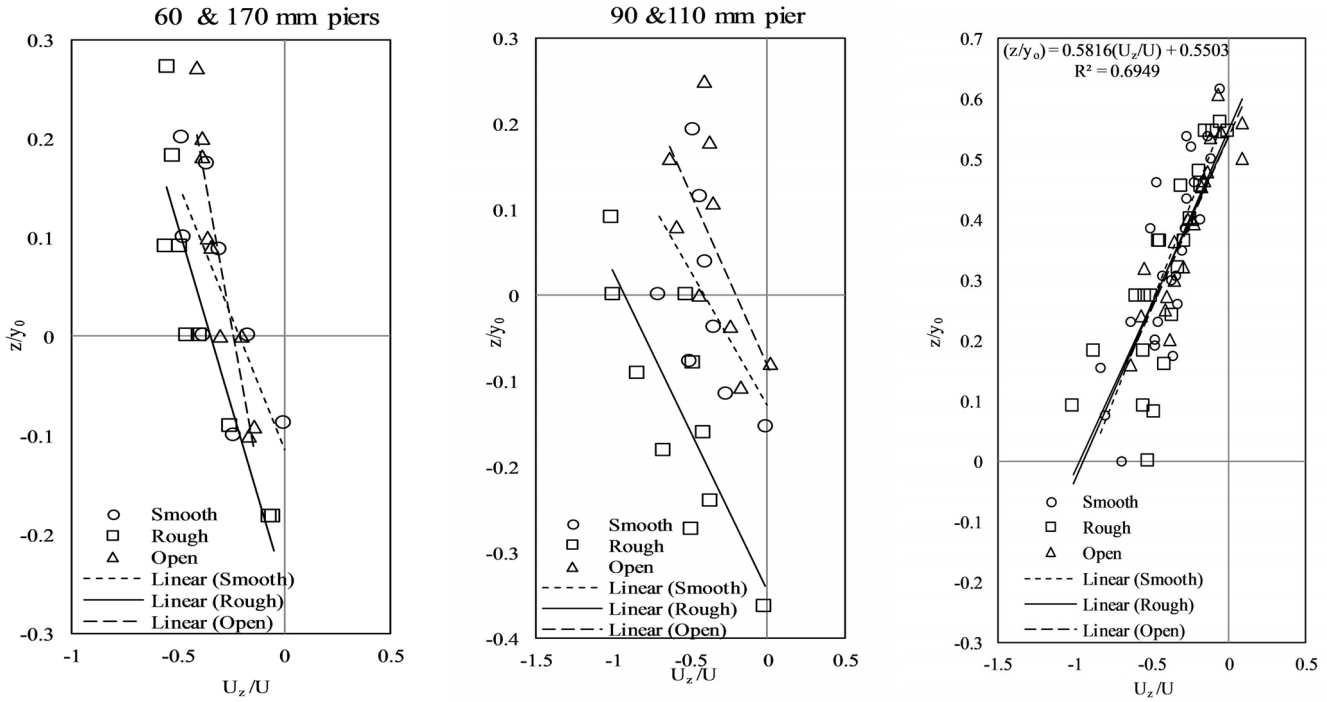

Fig. 10. a) Vertical velocity component (U_z) of the 60- and 170-mm bridge piers from the scour hole up to the maximum velocity locale under open, smooth and rough-covered flow covers; **b)** Vertical velocity component (U_z) of the 90- and 110-mm bridge piers from the scour hole up to the maximum velocity locale under open, smooth and rough-covered flow covers; **c)** Vertical velocity component (U_z) of all the bridge piers from the maximum velocity locale toward the free surface under open, smooth and rough-covered flow covers.

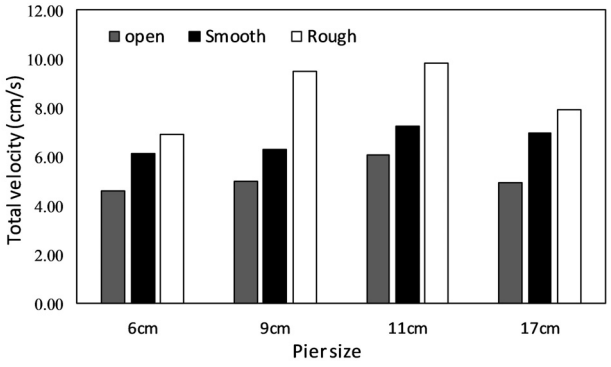

Fig. 11. Scour hole velocity profiles for velocity magnitude under open, smooth and rough ice cover for D_{50} = 0.47 mm for the lowest discharge.

conditions, there is more potential for sediment transport due to the higher kinetic energy than in the open channel and smooth ice-covered flow conditions.

3) Similar to the observations made for the velocity profile**,** for the 90 mm and 110 mm bridge piers in the first sand box, exposed to nearly the same flow depth and approaching flow velocity, the vertical turbulent intensities is higher for 110 mm than 90 mm pier under all forms of flow cover. Similar results were obtained for the 60 mm and 170 mm bridge piers in the second sand box with the 170 mm pier having higher values than the 60 mm pier under all flow cover conditions. The results show the turbulent intensity increases with pier size. The above statement can also be generalized for TKE. Therefore, it can also be concluded that, under nearly the same flow condition, the maximum value of turbulence kinetic energy occurs at a larger diameter pier.

CONCLUSIONS

In this paper, three-dimensional velocity components along with scour hole development patterns were measured around four pairs of bridge piers in channel bed with three non-uniform bed materials under open channel, smooth ice-covered, and rough ice-covered flow conditions. Following milestones of the experimental results are drawn from this study:

1) Experimental results showed that the local scour around side-by-side bridge piers was greater than that around a singular bridge pier. However, regardless of the flow condition (either open flow or ice-covered flow conditions) and the number of piers (either singular or side-by-side piers), the maximum scour depth occurred at the upstream front face of the bridge pier in which the horseshoe vortex and down-flow velocity coexist and were the strongest. On the other hand, the least amount of scour occurred behind the pier for both types of bridge arrangements regardless of flow cover. In terms of the impact of ice cover, the maximum scour depth was clearly the greatest under rough covered flow condition. Results also indicated that more sediment deposited at the downstream side of side-by-side bridge piers comparing to that of singular bridge pier.

2) The streamwise velocity component (U_x) was the lowest inside the scour hole and increased toward the free surface which gave a reversed C-shaped profile pattern. The negative values of U_x within the scour hole was an indication of reversal flow happening due to the presence of horseshoe vortex. In terms of velocity magnitude, the streamwise velocity under rough covered condition was generally greater than those under smooth covered and open channel conditions.

3) The vertical velocity distribution (U_z), which is a representative of the strength of downfall velocity, was the greatest under rough covered condition. Generally, The U_z values were negative inside the scour hole which indicated that U_z is down-

ward inside the scour hole. Under rough covered condition, the values of downward velocity component were higher which caused greater downfall velocities and ultimately greater scour depths. From the bed level before scouring process started, U_z tended to change its direction upward as it moved towards the water surface.

4) In terms of the lateral velocity component (U_y), there was not any meaningful pattern. Besides, there was no significant difference in velocity field if the channel bed material is different.

5) The experimental results showed that the locale of maximum velocity is closer to the bed under rough ice-covered flow conditions which was in a good agreement with the previous studies.

6) Regardless of flow cover, the vertical turbulent intensity was highest exactly over the channel bed and diminished towards the flow surface which implies that the shear stress is strongest on the channel bed causing sediment to be transported at a higher rate. Besides, under the same flow conditions, the value of turbulence kinetic energy increased with pier size.

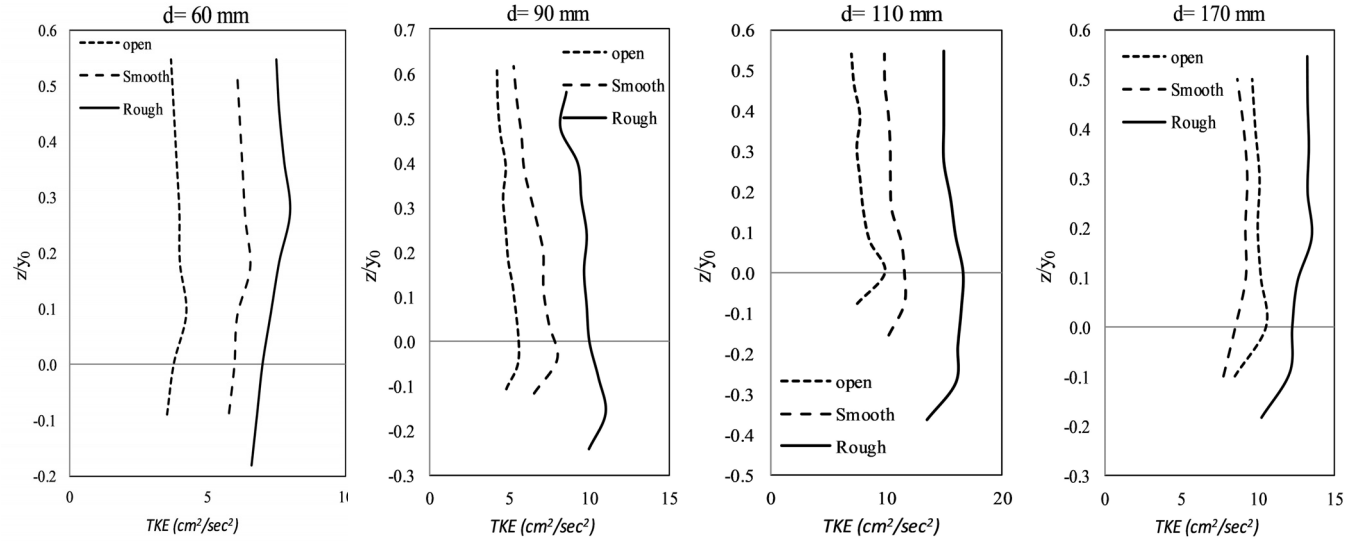

Fig. 12. Distributions of the turbulent kinetic energy at the upstream of the piers.

REFERENCES

Ahmed, F., Rajaratnam, N., 1998. Flow around bridge piers. Journal of Hydraulic Engineering, 124, 3, 288–300.

Ataie-Ashtiani, B., Aslani-Kordkandi, A., 2012. Flow field around side-by-side piers with and without a scour hole. European Journal of Mechanics-B/Fluids, 36, 152–166.

Beheshti, A.A., Ataie-Ashtiani, B., 2009. Experimental study of three-dimensional flow field around a complex bridge pier. Journal of Engineering Mechanics, 136, 2, 143–154.

Beltaos, S., 2007. River ice breakup processes: recent advances and future directions. Canadian Journal of Civil Engineering, 34, 6, 703–716.

Dey, S., Raikar, R., 2007. Clear-water scour at piers in sand beds with an armour layer of gravels. Journal of Hydraulic Engineering, 133, 703–711.

Ettema, R., Braileanu, F., Muste, M., 2000. Method for estimating sediment transport in ice-covered channels. Journal of Cold Regions Engineering, 14, 3, 130–144.

Ettema, R., Melville, B.W., Constantinescu, G., 2011. Evaluation of bridge scour research: Pier scour processes and predictions. Transportation Research Board of the National Academies, Washington, DC.

Fugate, D.C., Friedrichs, C.T., 2002. Determining concentration and fall velocity of estuarine particle populations using ADV, OBS and LISST. Continental Shelf Research, 22, 11–13, 1867–1886.

Golden Software, 1999. Surfer User's Guide: Contouring and 3D Surface Mapping for Scientists and Engineers. Golden Software, Inc., 809, 14th Street, Golden, CO 80401-1866.

Graf, W., Istiarto, W., 2002. Flow pattern in the scour hole around a cylinder. Journal of Hydraulic Research, 40, 1, 13–20.

Galan, A., Simarro, G., Fael, C., Cardoso, A.H., 2019. Clear water scour at submerged pile groups. International Journal of River Basin Management, 17, 1, 101–108.

Gautam, P., Eldho, T.I., Mazumder, B.S., Behera, M.R., 2019. Experimental study of flow and turbulence characteristics around simple and complex piers using PIV. Experimental Thermal and Fluid Science, 100, 193–206.

Hafez, Y.I., 2016. Mathematical modeling of local scour at slender and wide bridge piers. Journal of Fluids, Article ID 4835253. http://dx.doi.org/10.1155/2016/4835253.

Hains, D.B., Zabilansky L., 2004. Laboratory test of scour under ice: data and preliminary results. Cold Regions Research and Engineering Laboratory, ERDC/CRREL TR-04-09, Hanover, NH, USA.

Hirshfield, F., 2015. The impact of ice conditions on local scour around bridge piers. PhD Thesis. University of Northern British Columbia, Prince George.

Hodi, B., 2009. Effect of blockage and densimetric froude number on circular bridge pier scour. M.A.Sc. Thesis. Department of Civil and Environmental Engineering, Faculty of Engineering, University of Windsor, Windsor, Ont.

Kumar, A., Kothyari, U.C., 2011. Three-dimensional flow characteristics within the scour hole around circular uniform and compound piers. Journal of Hydraulic Engineering, 138, 5, 420–429.

Melville, B.W., Sutherland, A.J., 1988. Design method for local scour at bridge piers. Journal of Hydraulic Engineering, 114, 10, 1210–1226.

Melville, B.W., Chiew, Y.M., 1999. Time scale for local scour at bridge piers. Journal of Hydraulic Engineering, 125, 1, 59–65.

Melville, B.W., Coleman, S.E., 2000. Bridge Scour. Water Resources Publication.

Muste, M., Braileanu, F., Ettema, R., 2000. Flow and sediment transport measurements in a simulated ice-covered channel. Water Resources Research, 36, 9, 2711–2720.

Namaee, M.R., Sui, J., Whitcombe, T., 2017. A revisit of different models for flow resistance in gravel-bed rivers and hydraulic flumes. International Journal of River Basin Management, 15, 3, 277–286.

Namaee, M.R., Sui, J., 2019a. Impact of armour layer on the depth of scour hole around side-by-side bridge piers under ice-covered flow condition. Journal of Hydrology and Hydromechanics, 67, 3, 240–251.

Namaee, M.R., Sui, J., 2019b. Local scour around two side-by-side cylindrical bridge piers under ice-covered conditions. International Journal of Sediment Research, 34, 4, 355–367.

Namaee, M.R., Sui, J., Wu, P., 2019. Experimental Study of Local Scour around Side-by-Side Bridge Piers under Ice-Covered Flow Conditions. In: Fluvial Processes and Forms-Dynamics, Delineation and Conservation. IntechOpen. http://dx.doi.org/10.5772/intechopen.86369.

Mohammed, T.A., Noor, M.J.M.M., Ghazali, A.H., Yusuf, B., Saed, K., 2007. Physical modeling of local scouring around bridge piers in erodible bed. Journal of King Saud University-Engineering Sciences, 19, 2, 195–206.

Qadar, A., 1981. The vortex scour mechanism at bridge piers. Part 2. Proceedings of the Institution of Civil Engineers, 71, 3, 739–757.

Rickenmann, D., Recking, A., 2011. Evaluation of flow resistance in gravel□bed rivers through a large field data set. Water Resources Research, 47, 7, Article Number W07538.

Robert, A. Tran, T., 2012. Mean and turbulent flow fields in a simulated ice-covered channel with a gravel bed: some laboratory observations. Earth Surface Processes and Landforms, 37, 951–956.

Sontek, A.D.V., 1997. Operation manual, firmware version 4.0. Sontek, San Diego.

Sontek, 2001. ADV operation manual. 1st Ed. Sontek Inc., San Diego.

Sheppard, D.M., Melville, B., Demir, H., 2013. Evaluation of existing equations for local scour at bridge piers. Journal of Hydraulic Engineering, 140, 1, 14–23.

Sutherland, A.J., 1986. Reports on bridge failure. RRU Occasional Paper. National Roads Board, Wellington, New Zealand.

Sui, J., Wang, J., He, Y., Krol, F., 2010. Velocity profiles and incipient motion of frazil particles under ice cover. International Journal of Sediment Research, 25, 1, 39–51.

Unger, J., Hager, W.H., 2007. Down-flow and horseshoe vortex characteristics of sediment embedded bridge piers. Experiments in Fluids, 42, 1, 1–19.

Vijayasree, B.A., Eldho, T.I., Mazumder, B.S., Ahmad, N., 2019. Influence of bridge pier shape on flow field and scour geometry. International Journal of River Basin Management, 17, 1, 109–129.

Wardhana, K., Hadipriono, F.C., 2003. Analysis of recent bridge failures in the United States. Journal of Performance of Constructed Facilities, 17, 3, 144–150.

Wang, J., Sui, J., Karney, B., 2008. Incipient motion of non-cohesive sediment under ice cover – an experimental study. Journal of Hydrodynamics, 20, 1, 117–124.

Williams, P., Bolisetti, T., Balachandar, R., 2017. Evaluation of governing parameters on pier scour geometry. Canadian Journal of Civil Engineering, NRC Research Press, 44, 1, 48–58. DOI: 10.1139/cjce-2016-0133.

Williams, P., Balachandar, R., Bolisetti, T., 2018. Blockage corrections for pier scour experiments. Canadian Journal of Civil Engineering. http://doi.org/10.1139/cjce-2017-0563.

Wu, P., Hirshfield, F., Sui, J., 2014. Further studies of incipient motion and shear stress on local scour around bridge abutments under ice cover. Canadian Journal of Civil Engineering, 41, 892–899.

Wu, P., Balachandar, R., Sui, J., 2015a. Local scour around bridge piers under ice-covered conditions. J. of Hydraulic Engineering, 142, 1, Art. No. 04015038, 10.1061/(ASCE)HY.1943-7900.0001063.

Wu, P., Hirshfield, F., Sui, J., 2015b. Armour layer analysis of local scour around bridge abutment under ice covered condition. River Research and Applications, 31, 6, 736–746. DOI: 10.1002/rra.2771.

Wu, P., Hirshfield, F., Sui, J., 2015c. Local scour around bridge abutments under ice covered condition- an experimental study. International Journal of Sediment Research, 30, 39–47.

Wu, P., Balachandar, R., 2016. Local scour around bridge abutments including effects of relative bed coarseness and blockage ratio. Canadian Journal of Civil Engineering, 43, 1, 51–59.

Zabilansky, L.J., Hains, D.B., Remus, J.I., 2006. Increased bed erosion due to ice. In: 13th International Conference on Cold Regions Engineering, pp. 1–12. DOI: 10.1061/40836(210)16

Zhao, M., Cheng, L., Zang, Z.P., 2010. Experimental and numerical investigation of local scour around a submerged vertical circular cylinder in steady currents. Coastal Engineering, 57, 8, 709–721.

NOMENCLATURE

d: Pier diameter (mm)
D_{50}: 50th percentile particle diameter (mm)
G: Bridge spacing (m)
Fr: Upstream Froude number
Q: Volumetric flow discharge (m^3/s)
R: Hydraulic radius (m)
Re$_b$: Pier Reynold number
S: Longitudinal slope of the channel
TKE: Turbulent kinetic energy (J/kg)
U_z: Vertical velocity component (m/s)
U_x: Streamwise velocity component (m/s)
U_y: Span-wise velocity component (m/s)
U: Average approach velocity (m/s)
U^*: Shear velocity (m/s)
U_R: Velocity magnitude (m/s)
X: Longitudinal distance in the channel (m)
y_0: Approach flow depth (mm)
y_{max}: Maximum scour depth (mm)
z: Vertical distance from bed (m)
θ: Flow temperature (^{0}C)
v: Kinematic viscosity (m^2/s)

Received 15 July 2019
Accepted 17 December 2019